Wave-Powered Buoy Using an Axial Flux Generator and Spiral Spring Energy Storage

John K. Goebel[1,2] and Payton F. Domville[1]

[1]North Carolina State University, Electrical and Computer Engineering
[2]University of North Carolina at Chapel Hill, Biomedical Engineering

***Abstract*—The world's ocean serves as a major renewable energy source and creates the opportunity for harvesting the kinetic and potential energy associated with its waves. Specifically, wave surge and heave are often used for wave energy conversion into electric energy. This paper describes a heave wave-powered buoy that uses a spiral spring energy storage mechanism, spool for mooring cable, and an axial flux generator that produces a peak voltage of approximately 7.5 V at 115 rpm. The 115 rpm was determined from the maximum vertical velocity, 0.3925 m/s, of the buoy with a simplistic sinusoidal 1D heave motion model and wave with a period of 8 s and amplitude of 0.5 m. The entirety of the mechanical assembly, excluding mooring cable and the anchor, weighs 986.7 g and was deemed to be buoyant through volumetric analysis.**

***Index Terms*—Spiral Spring, Axial Flux Generator, Linear Generator, Wave Buoy, Renewable Energy**

I. Introduction

A. Background

Wave energy is a renewable energy source that is generated when wind, created from the sun's solar energy, moves across open surfaces of water and transfers energy through friction [1]. As wind energy increases, more kinetic energy is transferred to the ocean surface and larger waves result. When a wave passes a fixed position (perpendicular to horizontal wave motion), the water surface changes in height (potential energy), creating the opportunity for an energy harvesting system [2].

Wave energy converters (WECs) are designed to convert this kinetic and potential energy from waves into electric energy [3]. Because ocean waves generated by the wind are non-linear and chaotic, there is no single equation that fully describes or predicts their movement as a function of position and time. However, ocean wave motion is often treated as sinusoidal and can be characterized as a composition of sinusoidal functions with different amplitudes, phases, and frequencies.

Based on the motion of the wave, energy harvesting devices work in two primary ways: from the vertical motion (heave) or from the horizontal movement (fluctuation in ocean tide or surge) [3]. Technically, floating devices responding to real-world waves can be modeled with 6 degrees of freedom (DOF): surge, sway, heave, roll, pitch, and yaw. But, for the purposes of this project, we simplified the movement to include only wave heave.

Wave profile devices are a class of device that float on or near the ocean surface and whose size is comparable to the wave length [2]. The dimensions of our energy harvesting device are small relative to the incident wavelength, so the device can be treated as operating in the lumped regime. In other words, the wave does not vary much across the size of the device, and can be represented as a 1-DOF heave across the system.

B. Design Scenario

Given a simplistic and ideal wave scenario, the objective was to design a small energy-harvesting device capable of converting ocean wave energy into electrical energy.

C. Performance Objectives

The design was required to meet the following performance objectives:

- The device must float on the ocean surface, although it may be tethered to the ocean floor.
- It must provide a 5 VDC electrical output capable of charging a standard smartphone.
- The total system mass must not exceed 1.0 kg.

D. Wave Mechanics and 1-D model

For this model, the ocean wave motion was approximated with a sinusoidal function of the form $A\sin(\omega t)$. This was chosen as a first-order representation of vertical (heave) wave motion. The wave had an amplitude of $0.5\,\mathrm{m}$ and a period of $8\,\mathrm{s}$, which is defined as moderate, organized, and predictable wave motion [4][5]. The described wave's motion gives an angular frequency of:

$$\omega = \frac{2\pi}{T} = \frac{2\pi}{8} = 0.785\ \mathrm{rad/s}.$$

Thus, the vertical displacement of the buoy was modeled as:

$$x(t) = 0.5\sin(0.785t).$$

Taking the first and second derivatives gives the buoy velocity and acceleration:

$$v(t) = \dot{x}(t) = 0.3925\cos(0.785t),$$
$$a(t) = \ddot{x}(t) \approx -0.308\sin(0.785t).$$

While this first order model is useful as an approximation, a more accurate model involves the linear relationship described by [6]. Using a summation of forces in the vertical direction, including buoyancy, gravity, spring force, wave force, and damping, the buoy can be modeled as a one-dimensional mass-spring-damper around the system equilibrium [7]:

$$m\ddot{z} + c\dot{z} + (k_s)z = F_{\text{ext}},$$

where m is the buoy mass, c is the damping coefficient, k_s is the equivalent linear stiffness of the spiral spring, and F_{ext} is the external wave excitation force [6]. In this model, gravity and the static buoyant force are balanced at this equilibrium position. Hydrodynamic effects are not modeled explicitly.

E. Ideation Stages

1) Existing Solutions: When browsing the internet for existing solutions, we found a wide range of wave harvesting concepts. These systems employed mechanisms such as gear trains, pumps, pneumatic conversion, generators, dead weights, springs, flywheels, etc. all to convert the ocean's kinetic and potential energy into electrical energy. Some designs place the buoy or energy conversion device above the water surface, at the surface, or just beneath the ocean surface. Other systems separate the flotation component from the energy conversion component and distribute these systems in some combination between the ocean surface and floor. The conclusion from this survey was that there is no definitively correct or most efficient way to harvest wave energy, with each system having its own set of assumptions/simplifications.

2) Permanent Magnet Linear Generator: We initially considered a permanent magnet linear generator [8]. The concept began with a single magnet, attached to the buoy, moving through a stationary coil fixed to the ocean floor. This was later extended to a Halbach magnet arrangement with multiple magnets to increase the magnetic flux variation and improve induced voltage [9]. In both configurations, simulation results showed that with our wave's max velocity of 0.3925 m/s and small air gaps, the slow period of the ocean wave made it difficult to generate sufficient speed voltage to hit the goal of 5 Volts. Additionally, the stator or translator would need to have a length comparable to the wave height, 1 m, in order to induce voltage over the full vertical motion of the buoy. This made the concept less practical under the mass constraint of 1 kg.

3) Rack and pinion with gear train: After realizing that we needed to convert the relatively long vertical motion of the buoy, 1 m, into periodic rotational motion such that we could generate sufficient speed voltage of the magnet through the coil, we explored a rack and pinon with a gear train and slider mechanism. After several design versions, we considered configurations in which the rack was fixed either to the moving buoy or the ocean floor, with the pinion and gear train arranged in the opposite manner. However, this approach led to issues such like needing a long rack for the full stroke (plus its associated weight) and the complexity of a lightweight enclosure that would prevent saltwater from entering the gear train from the rack. We then considered using flexible bellows to encase the rack, while the rack was fixed to the ocean floor with the buoy moving up and down from the gravitational/buoyant force, but still this approach seemed to be too heavy for deep waters.

4) Generator with Spiral Spring: Finally, we settled on a buoyant system inspired from the internal mechanism of a badge reel. In this mechanism, the extension of the cord causes the spiral spring to wind and store mechanical energy which is then used to retract the cord when it is released. A similar idea is used in tape measures where a coiled spring works with a breaking mechanism to retract the tape after it is extended. Applying this idea to our design, we aimed to use a spiral spring to provide a downward force on the buoy in the negative heave direction (or towards the ocean floor) of which the buoy was moored.

II. Materials and Methods

A. Mechanical Enclosure

The mechanical enclosure was designed using SolidWorks. The objective of the enclosure was to provide a stable environment for the energy harvesting mechanisms (spiral spring, spool, bearings, and axial flux generator) within the buoy.

The design process began with the spiral spring, modeled with 17-7 PH stainless steel, as shown in Figure 1. The dimensions were estimated with an online spiral spring calculator [10]. The spring was designed with an inner diameter of 20 mm, an outer diameter of 80 mm, 7 turns, a strip width of 20 mm, and a thickness of 0.1 mm. A Young's modulus of 2.0×10^{11} Pa was assumed. The spring load was estimated as 0.308 N based on the peak inertial force for a 1 kg with the 1D heave sinusoidal motion. Using these parameters, the spring was calculated to produce an angular twist of 2910.6°,

required a total strip length of 1.09 m, and developed a bending stress of 739.2 MPa, which was a reasonable value for the selected material that is often used for high stress springs [11].

Fig. 1: The spiral spring was designed with seven turns and sized to provide sufficient angular deflection and restoring torque for the target vertical wave motion.

The spring design parameters were manipulated so that the available cord travel would exceed the target ocean displacement of 1 m in the vertical direction. A 1 mm diameter steel cord was wrapped around a spool with a radius of 85 mm. The theoretical cord travel is then given by:

$$s \approx r_{\text{wrap}}\theta \approx 4.32m,$$

where r_{wrap} is the spool wrap radius ($\approx OD_{spring}$) and θ is the spring rotation in radians. This value of travel is well above the 1 m wave model target. The corresponding cord force can be approximated from the spring torque as

$$F \approx \frac{M}{r_{\text{wrap}}},$$

which yielded approximately 0.308 N [10]. This indicates that the spring should provide sufficient restoring force to pull the buoy downward during operation.

After sizing the spring, the next step was designing an enclosure which placed the spring relative to the spool, Figure 2. While some spiral spring mechanisms place the spring adjacent to the spool on a separate shaft, we decided to place the spiral spring inside the spool itself to make the design more compact. In this configuration, one end of the spring is attached to a rod within the central shaft with a slit down the center for securing the spring. This inner shaft is not fixed to the spool itself but to an axial pin (within the shaft that rotates) which is then connected to the enclosure wall so it remains stationary. The other side of the spring is attached to the spool wall. As the spool rotates, the spring stores or releases energy from strain in the metal as one end of the spring is fixed to the spool and the other end is fixed to the stationary enclosure. This is the key mechanism that allows the buoys motion to be converted into rotational mechanical energy.

With an inner spool diameter of $85\,\text{mm}$, a spool width of $35\,\text{mm}$, and a radial depth of $7\,\text{mm}$, the approximate cable capacity can be estimated with a $1\,\text{mm}$ diameter cord, 7 winding layers, and 35 wraps per layer. The inner winding radius is $42.5\,\text{mm}$, and the outer winding radius is $49.5\,\text{mm}$, with an average winding radius of 46 mm. The total stored cable length is then approximately:

$$L \approx N_{\text{layers}}\, N_{\text{wraps/layer}}\, 2\pi r_{\text{avg}} \approx 70.8m$$

This cable capacity does not mean that the spring is meant to remain under strain over the full cable length. Rather, it shows that excess line can be held in the spool before the anchor is dropped to the ocean floor. Ideally, enough cable is released so that the anchor reaches the seabed before the spring becomes excessively tensioned, which would then risk pulling the buoy below the surface if the spring tension force is greater than the buoyant force.

To prevent the buoy from being pulled beneath the surface, the spring tension should remain less than the buoyant force:

$$F_{\text{spring}} \leq F_{\text{buoyant}}$$

One side of the spool is open-faced to allow for the insertion of the spiral spring, after which a lid with a central hole for for the 10 mm diameter and hollow shaft is attached with four M4 screws, Figure 2. Within the central shaft, an axial pin holds the center of the spring stagnant. On the opposite side, the spool includes a shaft and mounting plate used to attach the rotor of the axial flux generator.

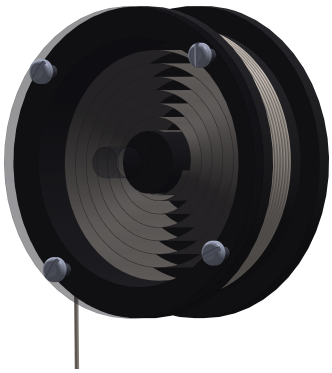

Fig. 2: The spiral spring is housed within the spool and a removable lid with screw fasteners are used to retain the spring within the enclosure while allowing torque to be transferred through the spool shaft.

Bearing supports were added on both sides of the spool to reduce the rotational friction and ensure that the spool does not misalign when it is winding/unwinding. The two support frames with bearings for the spool were mounted to the base of the enclosure. The bearings used were size 10-10, with a 10 mm bore diameter, 26 mm diameter, and 8 mm thickness. Again, the support structures were fixed to the bottom enclosure using M4 screws. The spool shaft was designed to have a clearance of 15 mm between the bearing and the spool to minimize stresses on the spool.

On the generator side, the spool-mounted plate was connected to the rotor using four M4 screws. The rotor consisted of a 1023 carbon steel plate with twelve NdFeB-35 permanent magnets. A separate support plate was used to mount both the stator and the enclosure base 4. The stator was constructed from a 1023 carbon steel plate and contained twelve sets of copper windings. There is approximately a 0.5 mm air gap between the magnets of the rotor and the stator. The spacing between the spool and the rotor was adjusted with the shaft length as to place the center of mass roughly near the center of the buoy Figure 3.

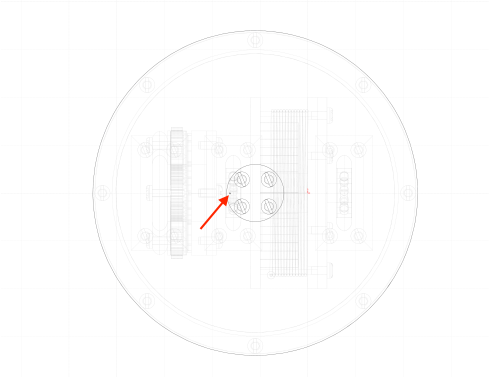

Fig. 3: Top-view SolidWorks model of the buoy assembly showing the center of mass with the red arrow. The image is taken with 20 mm grid spacing.

To allow the mooring cord to exit the enclosure while limiting seawater from getting into the enclosure, the spool shaft and cord were routed through the bottom of the enclosure with a rubber seawater gasket. This is an major simplification of strategy that would be required to keep saltwater out of the system.

The overall mechanical enclosure was designed as a cylindrical housing with a diameter of 150 mm and a height of 120 mm, giving it a bucket-like shape. Around the top edge of the enclosure, a circular flange extends outward and provides mounting points for eight M4 screws that attach the upper flotation structure, Figure 6.

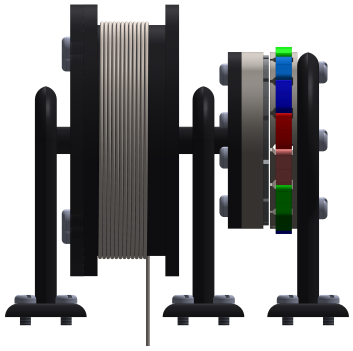

Fig. 4: Side-view of the spool, axial flux generator, and support structure. This view shows the relative placement of the spool, generator rotor and stator, and the support frames that are primarily for structural stability.

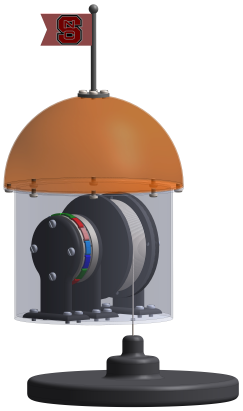

Fig. 5: The design integrates the upper flotation shell, spool, spiral spring energy storage mechanism, axial flux generator, support structure, and mooring connection within a cylindrical enclosure.

The top buoy was designed as a hollow swept hemispherical shell with a diameter of 170 mm. Both the main enclosure and buoy shell were modeled as hollow structures with a wall thickness of 2 mm to reduce total mass. The buoy base shell and top orange float were designed with simple cylindrical and half sphere shapes as to aid in the simple buoyancy analysis approach. Finally, at the top of the buoy, a small stand was mounted using four M4 screws to hold an NC State flag, Figure 5. The total mass for the assembly, excluding the mooring line and anchor was 986.7 g as shown in the BOM Table I in the Appendix.

B. Buoyancy Analysis

An extremely simplified approach was taken for the the buoyancy analysis. By Archimedes' principle, any

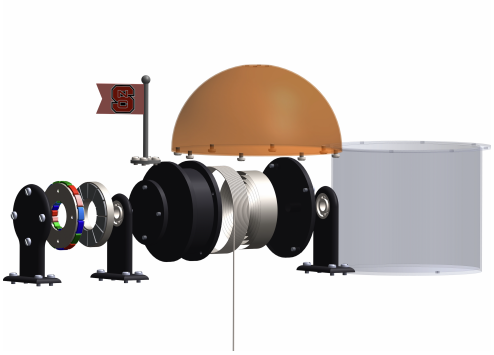

Fig. 6: Exploded SolidWorks view of the full buoy assembly.

object submerged in a fluid experiences an upward buoyant force equal to the weight of the fluid it displaces [12]. Therefore, the buoyant force can be determined by the volume of displaced water. The total mass of the buoy system was approximately $986.7\,\mathrm{g}$. The upper flotation section was modeled as a half-sphere shell with an inner radius of $85\,\mathrm{mm}$. The enclosed volume of a the half-sphere is given by

$$V = \frac{2}{3}\pi(r)^3 \approx 1.29 \times 10^{-3}\,\mathrm{m}^3.$$

Assuming seawater with a density of $1000\,\mathrm{kg/m^3}$, this corresponds to a displaced-water mass of approximately

$$m_{\text{displaced}} = \rho V \approx 1000(1.29 \times 10^{-3}) = 1.29\,\mathrm{kg}.$$

Since this displaced mass exceeds the buoy mass of $0.9867\,\mathrm{kg}$, the half-sphere flotation section alone provides enough buoyancy to float the system, even before including any additional buoyancy from the cylindrical section containing the electromechanical components which had an inner diameter of $148\,\mathrm{mm}$ and a height of $120\,\mathrm{mm}$. This additional volume gives margin for the buoy flotation during dynamic movement from heave and the spiral spring force.

For simplified dynamics, we want the buoyant force to be large relative to the system inertia so that the buoy more closely follows the 1-D wave motion and does not majorly deviate from the vertical water position. Many papers have explored this complex and non-linear relationship, which was not a focus for this project [6] [13] [14].

C. Initial Linear Flux Generator

Prior to the axial flux generator design, an initial concept based on a linear permanent magnet generator was developed and analyzed. The linear generator consisted of a center magnetic assembly and an outer coil structure.

1) Magnetic Assembly: The center assembly was constructed with four permanent magnets and three steel spacers arranged in alternating polarity along the axial direction. This alternating arrangement was chosen to maximize the number of flux reversals per unit length of translator travel, increasing the rate of change of flux linkage through the coil and therefore the induced voltage.

2) Coil Construction: The outer coil was parameterized based on the desired number of turns, number of layers, and wire diameter. The coil utilized $0.255\,\mathrm{mm}$ diameter copper wire wound to 200 turns over 10 layers. The coil height was determined by

$$h = N \cdot (2r_w),$$

where N is the number of turns and r_w is the wire radius. The coil outer radius was defined as

$$r_{\text{outer}} = a + r_w + (L \cdot d),$$

where a is the mean radius of the innermost winding layer, L is the number of layers, and d is the wire diameter. A hollow central bore of radius $a - r_w$ was subtracted to accommodate the sliding magnet assembly.

The total winding resistance was estimated from

$$R = \frac{\rho\,\ell}{A},$$

where the total conductor length was approximated as

$$\ell = 2\pi\left(a + \frac{d \cdot L}{2}\right) \cdot N \cdot L,$$

the conductor cross-sectional area as

$$A = \pi\left(\frac{d}{2}\right)^2,$$

and the resistivity of copper as $\rho = 1.68 \times 10^{-8}\ \Omega \cdot \mathrm{m}$. These parameters yielded an estimated coil resistance of approximately $87\ \Omega$.

3) Rationale for Design Transition: The primary limitation of the linear generator is geometric. To induce voltage over the full displacement of the wave, the coil length must be approximately equal to the peak-to-peak translator travel. Under the assumed wave model with $1\,\mathrm{m}$ of vertical displacement, this requires a coil on the order of $1\,\mathrm{m}$ in length. Even the shorter prototype coil with a length of $51\,\mathrm{mm}$ and outer diameter of approximately $45\,\mathrm{mm}$, already contributed substantially to the system mass budget coming in at approximately 650 grams, making a full-length coil infeasible within the $1\,\mathrm{kg}$ mass constraint.

A mechanical advantage mechanism, such as a rack-and-pinion stage to convert wave travel into multiple shorter translator strokes, was considered as a potential remedy. However, this approach introduced significant

added mechanical complexity, additional mass, and potential failure modes in a saltwater environment.

For these reasons, the design was transitioned to the axial flux generator described in the following section. The axial flux topology offers a more compact form factor, higher power density, and a natural integration with the developed buoy design.

D. Axial Flux Generator

1) Generator Construction: The axial flux generator was designed using Ansys RMxprt. The stator was configured as an `AXIAL_AC` machine type and the rotor as an `AXIAL_PM` type, with an air gap length of 0.5 mm between the rotor and stator faces.

The machine was constructed with 12 poles and 15 slots in a three-phase wye (Y) winding configuration. The stator core has an outer diameter of 65 mm, an inner diameter of 30 mm, a thickness of 10 mm, and a stacking factor of 0.95, and is composed of Steel_1010. The windings are double-layered with 400 conductors per slot of 32 AWG wire (0.203 mm wire diameter) and a coil pitch of 1. The resulting slot fill factor from the RMxprt solution was 61.55%. The rotor shares the same outer and inner diameters of 65 mm and 30 mm respectively, with a length of 8 mm and a stacking factor of 0.95, also composed of Steel_1010. The rotor core has a pole embrace of 0.9 and is fitted with NdFe35 permanent magnets of length 15 mm and thickness 2 mm.

2) Maxwell 3D Simulation Setup: Following the RMxprt design stage, the generator model was exported and analyzed in Ansys Maxwell 3D. Several modifications were made to the simulation setup to accurately model the generator operating as an energy harvester rather than a motor.

First, the excitation voltage was changed from the RMxprt preset value to zero. This ensures that all electrical output in the simulation is derived solely from induced EMF due to the relative motion between the rotor magnets and the stator windings that is, a change in flux linkage caused by the rotating permanent magnets. Setting a nonzero excitation would otherwise supply energy to the coils externally and obscure the true generation behavior.

Second, the rotational velocity in the motion setup was defined as a time varying function to model the angular velocity that results from the buoy's wave driven motion. While the effect of this variation is negligible at small simulation timescales, it was included for physical consistency.

All simulations were performed with time steps ranging from 0.5 ms to 5 ms depending on the analysis type. Coarser time steps were initially explored but produced suboptimal results. Since induced voltage is calculated as

$$\mathcal{E} = -\frac{d\Phi}{dt},$$

an excessively large time step relative to the rate of flux change leads to poor approximation of the instantaneous induced voltage. Finer time steps were therefore necessary to accurately resolve the induced waveforms.

3) Rectifier Circuit and Charging Model: After characterizing the generator in Maxwell 3D, the generator model was incorporated into a three phase rectifier circuit to evaluate its ability to charge a 5 V battery. The rectifier consists of six diodes arranged in a full bridge configuration, three on the positive rail and three on the negative rail, producing a rectified output waveform at twice the frequency of the input phase envelope.

The left side of the circuit, seen in Figure 7, represents the generator model, comprising the per phase induced voltage waveform, winding resistance, and winding inductance as extracted from Maxwell. The rectifier output was connected to a 5 V voltage source in series with a 0.1 Ω resistor, representing the terminal model of a 5 V battery under charge. The power delivered to the battery was computed by monitoring the current entering the positive terminal of this voltage source.

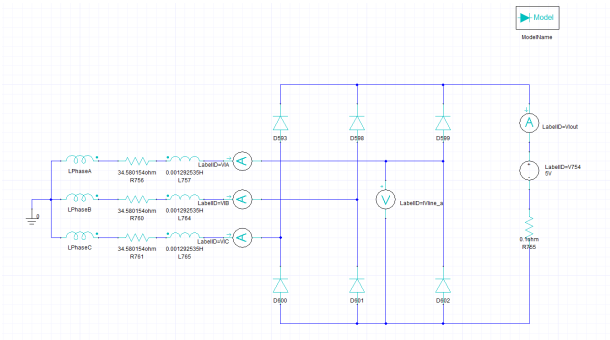

Fig. 7: schematic built in Maxwell Circuit for simulating the generators use for battery charging utlizing a 3 phase full wave rectifer circuit.

While the diodes, generator phases, and battery terminal are each modeled with basic non idealities, several second order effects are not captured, including diode forward resistance, junction capacitances, and thermal dissipation. Additionally, the present circuit topology does not include output filtering. A practical implementation would incorporate an RLC filter to suppress current and voltage ripple, and would ideally replace the simple rectifier with a dedicated charging circuit such as a constant-current/constant-voltage (CC/CV) topology with appropriate filtering for safely charging a lithium-ion battery.

III. Results

A. Linear Flux Generator

Electromagnetic simulation of the linear generator produced a peak open-circuit winding voltage of approximately 6.25 V (Figure 8) at the maximum expected translational velocity of 0.3925 m/s.

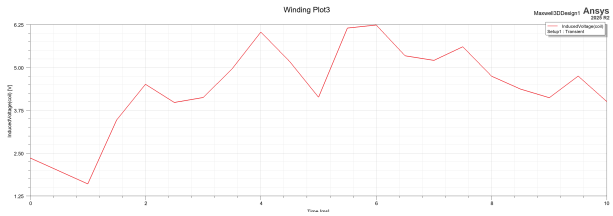

Fig. 8: Voltage measured across the winding of the linear flux generator, measured at a timestep of 0.5 ms, with a magnet assembly velocity of 0.3925 m/s

This also produces a corresponding winding current of approximately 75 mA through the winding, as shown in Figure 9.

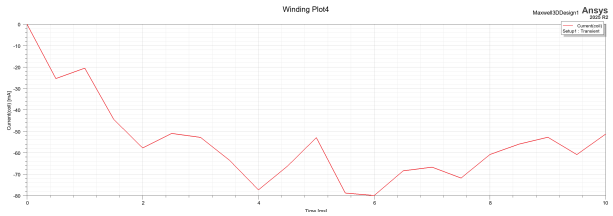

Fig. 9: Current measured through the winding of the linear flux generator, measured at a timestep of 0.5 ms, with a magnet assembly velocity of 0.3925 m/s.

An analysis of the magnetic flux changes were visualized using a B field plot for the magnetic assembly, Figure 10

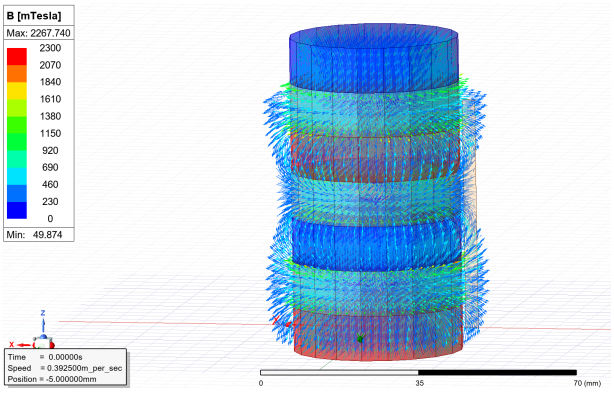

Fig. 10: 3D vector plot of the magnetic flux density throughout the magnetic assembly.

While the voltage target was nominally met, the coil length required to sustain induction over the full 1 m wave displacement rendered the design infeasible within the 1 kg mass constraint, motivating the transition to the axial flux topology.

B. Axial Flux Generator

1) RMxprt Solution: The RMxprt solution for the 12-pole, 15-slot axial flux generator yielded a slot fill factor of 61.55%, confirming that the 400-conductor, double-layer winding of 32 AWG wire (0.203 mm diameter) was geometrically feasible within the stator slot geometry.

2) Maxwell 3D Induced Voltage: Transient simulation in Maxwell 3D, with the excitation voltage set to zero and rotor motion driven by the wave-derived angular velocity profile, produced three-phase induced voltage waveforms in the stator windings as seen in Figure 11.

Fig. 11: Voltage induced across the three generator windings.

An example of the magnetic flux density for the axial flux generator can bee seen in Figure 12.

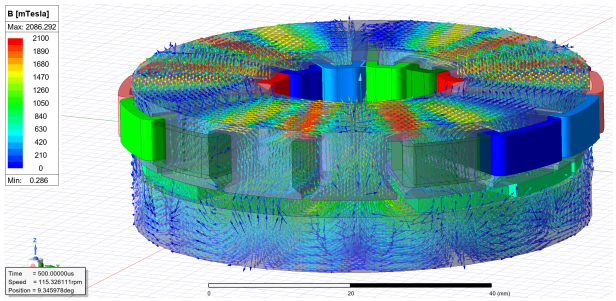

Fig. 12: 3D plot of the magnetic flux density through the axial flux machine.

3) Rectifier Output and Charging Performance: After connecting the Maxwell generator model to the three-phase full-bridge rectifier and the 5 V battery terminal model (0.1 Ω series resistance), the rectified output voltage seen in Figure 13 and battery charging current seen in Figure 14 were extracted. This results in a nominal power delivery to the battery at maximum velocity of approximately 0.5 Watts.

Fig. 13: Voltage measured across the axial flux generators phases when connected to the rectifier circuit.

Fig. 14: Current measured going into the 5V batteries positive terminal

IV. Conclusion

A. Application to Course and Measure of Success

This project has applications to the most recent machines coverage within the course and specifically the chapters on time varying magnetic fields and induced voltages. The electromagnetic principles that describe the behavior of the axial flux generator are the same set of Maxwell's equations taught in the course: Faraday's Law, Ampere's Law, and Gauss's Law for magnetic and electric fields.

One of the most fundamental relationships governing the electrical behavior, design, and output of the generator is Faraday's law of induction, expressed as

$$\mathcal{E} = -\frac{d\lambda}{dt},$$

where $\mathcal{E}$ is the induced voltage and λ is the total flux linkage through the winding. This single relationship underlies the operating principle of both generator topologies explored in this project, and reasoning about it in terms of cutting lines of magnetic flux (**"like a lawnmower"**) informed many of the key design decisions.

In the context of the axial flux generator, one of the primary design goals was to maximize the area of overlap between the permanent magnets and the stator windings. A larger magnet face area intersecting the coil increases the total flux linking the winding at any given rotor position, and therefore increases the magnitude of $d\lambda/dt$ as the rotor sweeps past each stator slot. This directly translates to a higher induced voltage per revolution. The same principle motivated the alternating polarity arrangement in the earlier linear generator design, where adjacent magnets of opposing polarity were used to maximize the number of flux reversals per unit length of translator travel, again exploiting Faraday's law to increase the rate of flux change through the coil.

Both partners agree that this project was a major success and thoroughly enjoyed the experience. Throughout the design process, we gained technical experience with real-world engineering tools, Solidworks and ANSYS, to develop a relatively creative solution.

B. Simplifications and Limitations

The wave model was extremely simplistic along with the governing dynamic equations that neglected real-world effects such as hydrodynamics. Additionally, motor simulations were conducted at 115 rpm which was determined from the maximum vertical velocity of the bouy, 0.3925 m/s.

Limitations of the mechanical design largely relate to cyclic deformation spiral spring. Given that wave harvesting device will most likely be deployed in the ocean for extended periods of time, it should be resilient throughout the entirety of its use. Extensive simulation or loading protocols using load frames should be done to determine optimal spring dimensions as to have the spring operate in a linear range for as many cycles as possible. When the spiral spring leaves the elastic region, we expect slack to build up in the cable and thus reduce the effectiveness of the generator system with an overall lower rpm. Additionally, the design would need to include sea-water gaskets as to prevent corrosion of the assembly.

With respect to power output, the generator is currently limited by the relatively low angular velocity achievable under direct wave-driven rotation, with a maximum of approximately 115 rpm. At this speed, the induced back-EMF is modest, constraining the deliverable output power. An improved design would incorporate a gear assembly between the spool and the generator rotor to step up the rotational velocity, which would increase the rate of flux change through the stator windings and allow for significant improvement in output power.

AI Usage Statement

AI Tools (ChatGPT and Claude) were used for textual, grammatical, and LaTeX editing with all content remaining original to the authors.

REFERENCES

[1] N. Pizzo, L. Deike, and A. Ayet, "How does the wind generate waves?" *Physics Today*, Nov. 2021. DOI: 10.1063/PT.3.4880. [Online]. Available: https://physicstoday.aip.org/features/how-does-the-wind-generate-waves.

[2] Alternative Energy Tutorials. "Wave energy devices, Devices that harness the oceans vast energy resource," Accessed: Apr. 17, 2026. [Online]. Available: https://www.alternative-energy-tutorials.com/wave-energy/wave-energy-devices.html.

[3] Oregon Sea Grant. "Wave energy 101," Oregon State University, Accessed: Apr. 17, 2026. [Online]. Available: https://seagrant.oregonstate.edu/ocean-renewable-energy/marine-energy/wave-energy.

[4] National Oceanic and Atmospheric Administration, *Waves*, https://www.noaa.gov/jetstream/ocean/waves, Accessed: 2026-04-17, Sep. 2023.

[5] SeaLegsAI, *Understanding wave height and period for boaters*, https://www.sealegs.ai/blog/understanding-wave-height-and-period, Published February 21, 2026. Accessed: 2026-04-17, Feb. 2026.

[6] Y. Li and Y.-H. Yu, "A synthesis of numerical methods for modeling wave energy converter-point absorbers," *Renewable and Sustainable Energy Reviews*, vol. 16, no. 6, pp. 4352–4364, Aug. 2012. DOI: 10.1016/j.rser.2011.11.008. [Online]. Available: https://www.sciencedirect.com/science/article/pii/S1364032111005351.

[7] Shim ReStackör. "Spring-mass-damper," Shim ReStackör, Accessed: Apr. 17, 2026. [Online]. Available: https://restackor.com/physics/response/spring-mass-damper.

[8] X. Niu, "Modeling and design analysis of a permanent magnet linear synchronous generator," Engineering System Design Lab, University of Illinois at Urbana-Champaign, Tech. Rep. UIUC-ESDL-2013-01, Aug. 2013. [Online]. Available: https://docs.systemdesign.illinois.edu/publications/Niu13a.pdf.

[9] K. B. Ahmed. "Permanent magnet linear generator (pmlg) design and fea simulation, Trade-off analysis of cogging force, back-emf, and halbach magnet arrangements," EMWorks, Accessed: Apr. 17, 2026. [Online]. Available: https://www.emworks.com/blog/motor-design/permanent-magnet-linear-generators-design-challenges.

[10] Calcdevice.com, *Spiral spring — online calculator*, https://calcdevice.com/spiral-spring-id11.html, Accessed: 2026-04-16, n.d.

[11] SSM Alloys, *17-7 ph stainless steel: Complete guide to properties, heat treatment & spring applications*, https://ssmalloys.com/17-7-ph-stainless-steel-complete-guide/, Published January 14, 2026. Accessed: 2026-04-16, Jan. 2026.

[12] Wikipedia contributors. "Archimedes' principle," Accessed: Apr. 17, 2026. [Online]. Available: https://en.wikipedia.org/wiki/Archimedes%27_principle.

[13] K. Khedkar and A. P. S. Bhalla, "A model predictive control (mpc)-integrated multiphase immersed boundary (ib) framework for simulating wave energy converters (wecs)," *Ocean Engineering*, vol. 260, p. 111 908, 2022. DOI: 10.1016/j.oceaneng.2022.111908. [Online]. Available: https://www.researchgate.net/publication/358271700_A_model_predictive_control_MPC-integrated_multiphase_immersed_boundary_IB_framework_for_simulating_wave_energy_converters_WECs.

[14] E. Katsidoniotaki, Y.-H. Yu, and M. Göteman, "Midfidelity model verification for a point-absorbing wave energy converter with linear power take-off," *International Marine Energy Journal*, vol. 5, no. 1, pp. 67–75, Jun. 2022. DOI: 10.36688/imej.5.67-75. [Online]. Available: https://docs.nlr.gov/docs/fy22osti/83489.pdf.

TABLE I: Bill of Materials for the Wave-Powered Buoy

Item No.	Part Number	Description	Mass (g)	Qty.	Total Mass (g)	Material
1	spiral spring	spring	17.83	1	17.83	17-7 PH stainless
2	spool	holds cord	124.27	1	124.27	High Density PE
3	spool lid	holds spring	38.12	1	38.12	High Density PE
4	bearing support	holds bearing	24.66	2	49.32	High Density PE
5	stator support	holds stator	39.14	1	39.14	High Density PE
6	rotor steel	rotor body	162.83	1	162.83	1023 carbon steel
7	rotor magnet	magnet	2.52	12	30.24	NdFeB-35
8	stator steel	holds coils	141.91	1	141.91	1023 carbon steel
9	stator coils	windings	4.54	12	54.48	copper
10	bottom encasement	holds assembly	167.85	1	167.85	High Density PE
11	top buoy	orange floater	64.68	1	64.68	High Density PE
12	flag	NC Flag	9.01	1	9.01	High Density PE
13	M4x0.7x5	pan-head screw	0.78	12	9.36	alumina
14	M4x0.7x8	pan-head screw	0.92	20	18.40	alumina
15	M4x0.7x10	pan-head screw	1.02	4	4.08	alumina
16	AFBME 20.1 -10-10 Full DE NC Full_68	bearings	2.59	2	5.18	n/a
17	gasket	cord/seawater	2.51	1	2.51	rubber
18	electronics/charging module	various electronics	50.00	1	50.00	various
19	mooring cord	1 mm dia. cord	n/a	n/a	n/a	316 Stainless Steel
20	anchor	anchor	n/a	n/a	n/a	316 Stainless Steel
				Total Mass	**986.70**	

V. APPENDIX